Materials Science in Semiconductor Processing 27 (2014) 865–872

Contents lists available at ScienceDirect

Materials Science in Semiconductor Processing

journal homepage: www.elsevier.com/locate/mssp

ZnSe nanoparticles of different sizes: Optical and photocatalytic properties

Bo Feng [a], Jian Cao [a], Donglai Han [b], Hongtao Liang [a], Shuo Yang [b], Xiuyan Li [a], Jinghai Yang [a]

[a] Key Laboratory of Functional Materials Physics and Chemistry of the Ministry of Education, Jilin Normal University, Haifeng Street no. 1301, Siping 136000, PR China

[b] Key Laboratory of Excited State Physics, Changchun Institute of Optics, Fine Mechanics and Physics, Chinese Academy of Sciences, 3888 Eastern Nan-Hu Road, Changchun 130033, PR China

ARTICLE INFO

Available online 18 September 2014

Keywords:
ZnSe
Nanoparticles
Optical properties
Photocatalysis

ABSTRACT

ZnSe nanoparticles (NPs) with different sizes from 7 to 21 nm were successfully prepared by a solvothermal method in the absence of surfactants. X-ray diffraction, transmission electron microscope, and photoluminescence were used to study the effect of reaction time on the sizes and optical properties of ZnSe NPs. The XRD analysis revealed that all the samples were the cubic zinc-blende structure. The particles size increased from 7 to 21 nm with increasing reaction time. The room-temperature PL spectra showed that the near-band-edge emission peak displayed an abnormal red-shift ranging from 472 to 479 nm when the particle size decreased from 21 to 7 nm, and the intensity of the peak decreased. The photocatalytic activities of the ZnSe NPs of different sizes were also investigated. The ZnSe NPs with smaller particle size had better photocatalytic activities than that with larger particle size for the degradation of Rhodamine B under UV radiation. And the photodegradation of Rhodamine B catalyzed by the ZnSe nanoparticles was a pseudo-first-order reaction.

1. Introduction

Owing to the unique mechanical, chemical, physical, biological and specific surface area properties, the nanomaterials have been applied as nanostructures, nanoelectronics, nanophotonics, nanobiomaterials, etc. In the last decade, a large variety of nanomaterials and devices with new capabilities have been generated employing NPs. The NPs possess unique optical and electronic properties which have not been observed in the corresponding bulk samples. Owing to a significant increase in the fraction of surface atoms and the prominent role of the surface effects, not only the optical properties but also other characteristics of materials become dependent on the size and shape of NPs. Therefore, it is extremely important to control the size of the NPs in order to obtain the desired physical properties. ZnSe is an important II–VI semiconductor with a room-temperature bulk bandgap of 2.67 eV (465 nm). ZnSe-based nanostructures have been the subject of intense interest in view of their wide-ranging applications such as light-emitting diodes (LEDs), blue light-emitting lasers, and photodetectors [1–6] owing to significantly large exciton binding energy (21 meV [7]) compared to GaAs (4.2 meV [8]). Semiconductor nanoparticles such as ZnSe and CdSe are very important materials owing to their crystal size-dependent electronic structure. The electronic structure leads to materials with tunable electrical or optical properties. For example, ZnSe has

E-mail addresses: fengbosiping@126.com (B. Feng), jhyang1@jlnu.edu.cn (J. Yang).

http://dx.doi.org/10.1016/j.mssp.2014.08.027
1369-8001/

attracted significant attention for its size-selective intense UV-blue emission, [9] which has not yet been observed in its other family members such as ZnS, CdS, and CdSe. ZnSe has been studied to a lesser extent compared to its "closest kin", CdS, CdSe, and ZnS. The various synthesis routes have been reported for the preparation of ZnSe NPs, mainly focusing on their structural characterization and rarely on their PL and photocatalytic properties [10,11]. For example, Deshpande successfully synthesized ZnSe NPs of different sizes by a simple and inexpensive low-temperature (~80 °C) wet chemical method [10]. Li et al. found that microwave irradiation power affected the sizes and shapes of ZnSe materials because of the movement and polarization of amine molecules under the rapidly changing electric field in a microwave reactor [11]. There are few reports on the comparison of the PL properties of ZnSe NPs of different sizes. Moreover, a good optoelectronic device should not only have high luminous efficiency, high thermostability, and low threshold of luminescence, but also can be tuned effectively. The way to adjust PL emission location plays a significant role in the optoelectronic application of ZnSe nanostructures. Until now, although the PL emission location can be adjusted via doping different elements to ZnSe nanostructures [12–15], it is relatively difficult to fabricate element-doped ZnSe nanostructures. In contrast, it may be easier to synthesize different sizes of the ZnSe NPs to control the location of the near-band-edge (NBE) emission.

Organic dyes have been widely used in textile, food, and paint industries, and a significant discharge of dye wastewater has caused significant environmental and health problems. The traditional purification procedures such as coagulation, filtration, microbial degradation, membrane separation, sedimentation, and adsorption have been used to treat dye wastewater [16,17]. However, these methods suffer from a disadvantage; the organic pollutants are often transferred to another collecting phase and do not get degraded to nontoxic substances completely [18]. In the last decades, semiconductors with photocatalytic properties have attracted worldwide attention because of their ability to completely eliminate the pollutants in wastewater [19]. Among various semiconductor materials, ZnSe has a great potential as a photocatalyst because of its suitable band gap [20,21]. For example, Zhang et al. reported that hollow ZnSe microspheres constructed from ZnSe nanoparticles were prepared via a facile hydrothermal reaction. And the ZnSe hollow microspheres displayed a high photocatalytic activity in the photodegradation of methyl orange at room temperature [22]. To the best of our knowledge, ZnSe NPs with a tunable and stable emission in the visible spectral region and their photocatalytic properties have rarely been reported.

In this paper, ZnSe NPs were synthesized by an easy controlled solvothermal method, and different sizes of the ZnSe NPs were obtained by simply varying the reaction time. This method provided a convenient, low-cost, and environment-friendly route for synthesizing ZnSe NPs under relatively moderate conditions. This method might be extended to the synthesis of other semiconductor nanostructures. The PL spectra and photocatalytic activities of ZnSe NPs with different sizes were studied in detail at room temperature.

2. Experimental

2.1. Preparation of ZnSe NPs

All chemicals were of analytical grade and used as received, without further purification. The synthesis of the ZnSe precursor was carried out using the following procedures: $Zn(NO_3)_2 \cdot 6H_2O$ (0.5 mmol) was dissolved in 30 ml of EDTA solution. The selenium powder (99.95%) (0.5 mmol) was dissolved in 30 ml of NaOH solution. After stirring for 1 h, both were added into one beaker. Then after stirring for a further hour, the mixed solution was transferred into the 80-ml Teflon-lined autoclave. The autoclaves were sealed and heated at 180 °C for 10 h (Sample C), 20 h (Sample B) and 30 h (Sample A), respectively. After the reaction, the autoclaves were cooled to the room temperature. The products were washed with ethanol and deionized water several times and then separated by centrifugation. They were then dried at 60 °C for 1 h to obtain the precursors. Finally, the precursors were annealed at 300 °C for 2 h to get the yellow ZnSe samples.

2.2. Characterization

X-ray diffraction (XRD) pattern was collected on a MAC Science MXP-18 X-ray diffractometer using a Cu target radiation source. Transmission electron micrograph (TEM) was taken with a JEM-2100 electron microscope. The specimen was prepared by depositing a drop of the dilute sample solution of the sample in 2-propanol on a carbon-coated copper grid and drying at room temperature. Energy dispersive x-ray analysis (EDAX) system attached to the SEM was employed to analyze chemical composition. The PL measurement was carried out at room temperature, using 325 nm as the excitation wavelength, and a He–Cd Laser as the excitation source.

The photocatalytic activity measurements are as follows: a reaction system that used the as-synthesized products as catalysts and including the Rhodamine B (RhB) aqueous solutions, was magnetically stirred in the dark until reaching the adsorption equilibrium of the RhB for the catalyst before exposure to UV irradiation from a 250 W high-pressure Hg lamp (centered at 365 nm). After exposure to the radiation for different intervals, the UV–vis spectrophotometer was used to determine the solution concentration of RhB at room temperature (UV-5800PC, Shanghai Metash Instruments Co., Ltd).

The degradation efficiency of the photocatalyst can be defined as follows:

$$\text{Degradation}\ (\%) = (1 - C/C_0) \times 100\%,$$

where C_0 is the initial concentration of RhB and C is the residual concentration of RhB at different illumination intervals.

The photodegradation of RhB follows pseudo-first-order kinetics, which can be expressed as follows:

$$\ln(C_0/C) = kt,$$

where k (min^{-1}) is the degradation rate constant.

3. Results and discussion

Fig. 1(a–c) shows the XRD patterns of the samples (A–C). The peaks are assigned to the diffractions from (111), (220), (311), (400), and (331) planes of the cubic zinc blende phase of ZnSe, which are in complete agreement with the PDF card ($F\bar{4}3m$, JCPDS file #37-1463). Moreover, no diffraction peaks from Zn or other impurities are observed within the detection limit. With the increase in the reaction time, all the peaks become stronger and sharper, indicating that the crystallization becomes better and the average crystalline grain size of the ZnSe NPs becomes bigger. The grain size of the crystallites (mean crystallite diameter, d) of as-obtained product was calculated using Scherrer's formula of peak width:

$$d = (0.9\lambda)/\beta \cos\theta$$

where λ is the wavelength of X-ray used (0.15418 nm in the present case), β is the full width in radiation at half-maximum of the peak, and θ is the Bragg angle of the X-ray diffraction peak. Calculation made on these peaks gave a value of 7.2 nm, 15 nm and 20.5 nm for the average crystallite diameter of the as-prepared ZnSe nanoparticles obtained at 10 h, 20 h and 30 h, respectively, which was close to the value measured by the TEM. The lattice constant (a) and volume of lattice (V) are listed in Table 1.

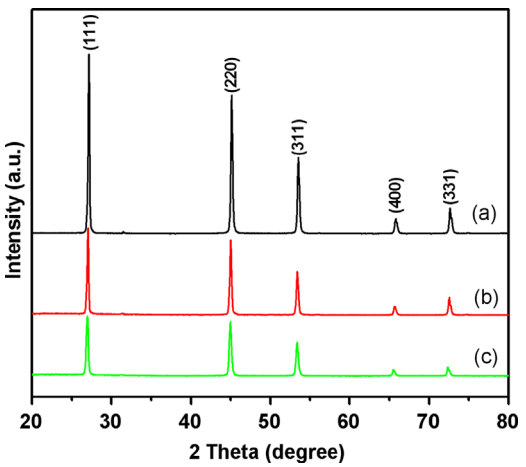

Fig. 1. XRD patterns of ZnSe NPs, Sample A (a), Sample B (b), and Sample C (c).

Table 1
Cell constant (a) and volume of lattice (V) of the samples.

Sample	Reaction time (h)	a (nm)	V (nm^3)
A	30	0.5673	0.1826
B	20	0.5687	0.1839
C	10	0.5696	0.1848

The lattice constant a of the three samples is slightly larger than the standard value of 5.668 Å, indicating that all the samples are under tensile strain.

Fig. 2 shows the TEM images of Sample C (a and b) and Sample A (c and d), indicating that the NPs are formed with a spherical shape. The reaction time is found to influence the particle size of the ZnSe NPs. The average particle size is approximately 7.0 nm as shown in Fig. 2(a), and approximately 21 nm as shown in Fig. 2(c). Fig. 2(b) and (d) shows the high-resolution TEM (HRTEM) micrographs of ZnSe, evidencing the highly crystalline nature of the samples. The HRTEM images show well-defined lattice planes reflecting a high degree of crystallinity within each single crystal. The observed interplanar distance of 0.33 nm is in agreement with the ZnSe zinc blende structure with a distance of 0.327 nm for the (111) planes (JCPDS-37-1463). The regular behavior of the lattice fringes inside the nanocrystal further confirms the good crystallinity nature of ZnSe NPs. And, the synthesized particle size has a certain distribution. The corresponding particle size distributions are shown in Fig. 2(e) and (f). The particle size is in the range of 6.0–8.0 nm for the sample obtained at 10 h, and the particle size is in the range of 20.0–24.0 nm for the sample obtained at 30 h. The EDAX analysis of the ZnSe NPs is shown in Fig. 2(g) (Sample C) and (h) (Sample A), respectively, indicating that both samples are composed of the elements Zn and Se (other peaks arise from the Au).

The room temperature PL spectra of the as-synthesized ZnSe NPs are shown in Fig. 3(A). The PL emission peak position and intensity of ZnSe NPs are strongly related to the particle size. Fig. 3(A) (black line) shows that for the ZnSe NPs (21 nm), the PL spectrum contains a strong emission peak at 472 nm and a weak defect-related emission band extending from 600 to 650 nm. The emission peak at 472 nm is usually attributed to the NBE emission of ZnSe, namely, the recombination of the free excitons (FXs) [23]. Fig. 3(A) (b) and (c) shows that for the ZnSe NPs (Samples B and C), the NBE emission peak first red-shift to 477 nm, and then to 479 nm. Moreover, the emission intensity decreases significantly. Furthermore, for the NPs (Sample C), the intensity of the defect-related emission band extending from 500 to 600 nm increases significantly. The large amount of amorphous particles in the ZnSe NPs (Sample C) would cause some defect states, which quench the luminescence, thus leading to a significant deterioration in the band-edge luminescence [24]. The position of the NBE emission peak shows a red-shift ranging from 472 to 479 nm with decreasing particle size from 21 to 7 nm. However, the low defect-related emission band becomes broader and stronger when the particle size reaches 7 nm. Through careful analysis, we propose that the surface band bending due to the large surface-to-volume ratio in ZnSe NPs is responsible for the abnormal phenomena in the PL spectrum of ZnSe NPs with the particle size from 21 to 7 nm. Both indirect and direct recombination will contribute to the NBE emission. Although the ZnSe nanomaterials are usually n-type, both donor- and acceptorlike states are present within the band gap. In this case, some donor electrons in the conduction band will reduce their energy by occupying

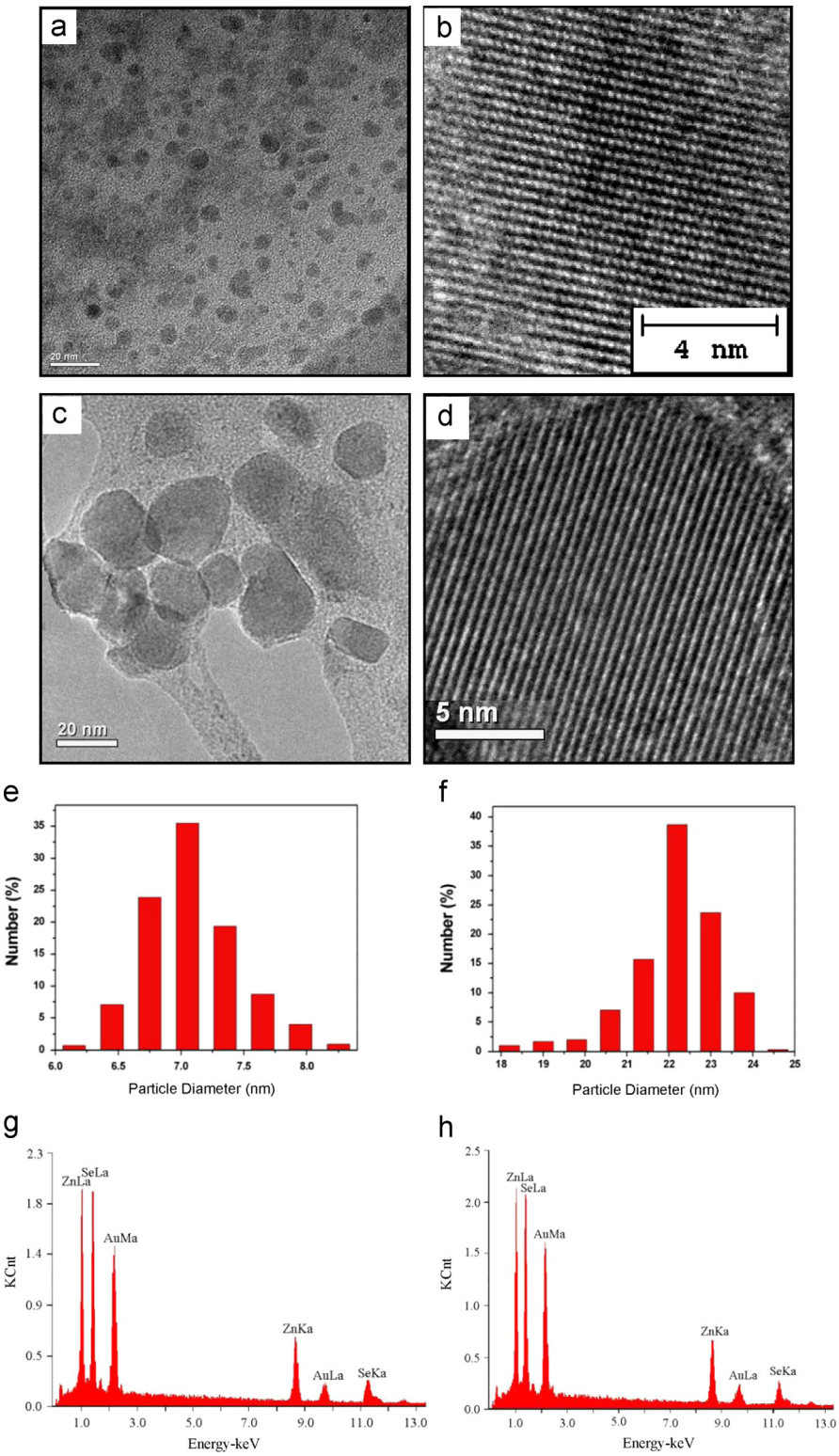

Fig. 2. TEM image (a), HRTEM image (b), particle size distributions (e), EDAX (g) of ZnSe NPs (Sample C), and TEM image (c), HRTEM image (d), particle size distributions (f), EDAX (h) of ZnSe NPs (Sample A).

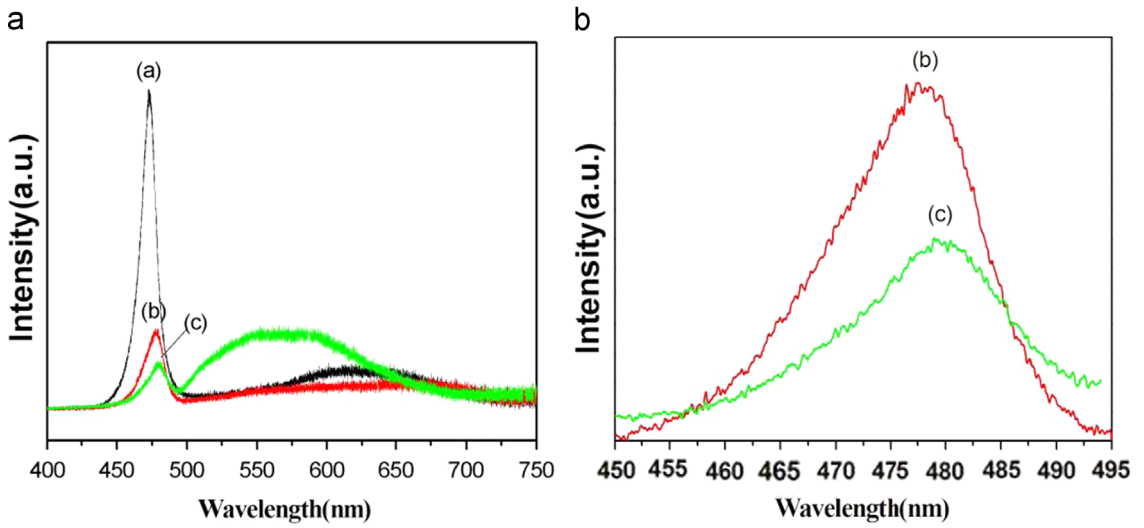

Fig. 3. (A) PL spectrum of ZnSe NPs with different particle sizes, Sample A (a), Sample B (b) and Sample C (c), (B) the enlarged NBE emission peak of ZnSe NPs Sample B (b) and Sample C (c).

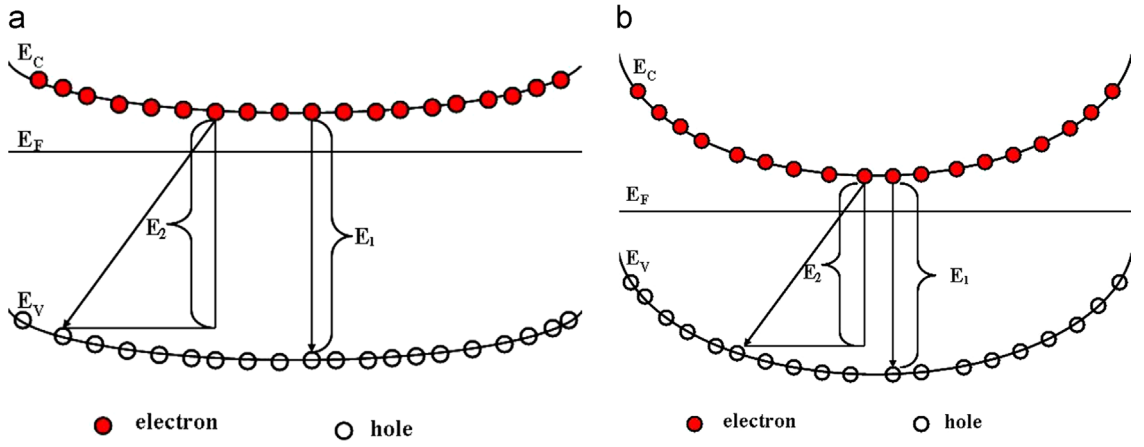

Fig. 4. Sketch of the energy band of ZnSe NPs with different type of surface depletion regions. (a) ZnSe NPs (21 nm) are partially depleted (b) ZnSe NPs (7 nm) are thoroughly depleted.

the acceptorlike surface states. ZnSe NPs exhibit intrinsic high surface-to-volume ratio, and they possess substantial defects, which give rise to the possibility that the electron can be trapped, thereby creating a surface built-in electric field. Consequently, the energy bands bend upwards as they approach the surface and finally results in a surface depletion layer, which will strongly influence the PL properties of ZnSe NPs [25,26]. Since ZnSe NPs usually have a very large surface–volume ratio, the band bending due to near surface on the PL process becomes more significant. The smaller the nanoparticle, the larger the surface–volume ratio and the stronger the band bending effect. In our case, the ZnSe NPs (7 nm) exhibit the intrinsic higher surface-to-volume ratio compared with the ZnSe NPs (21 nm). Hence, the band bending near surface will play an important role to influence the PL properties in ZnSe NPs (7 nm).

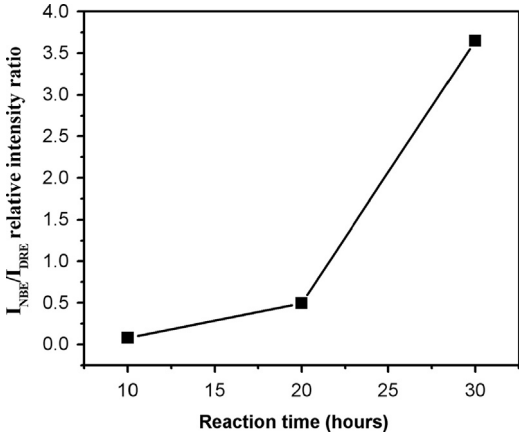

Fig. 5. The ratio of intensities I_{NBE}/I_{DRE} versus reaction time.

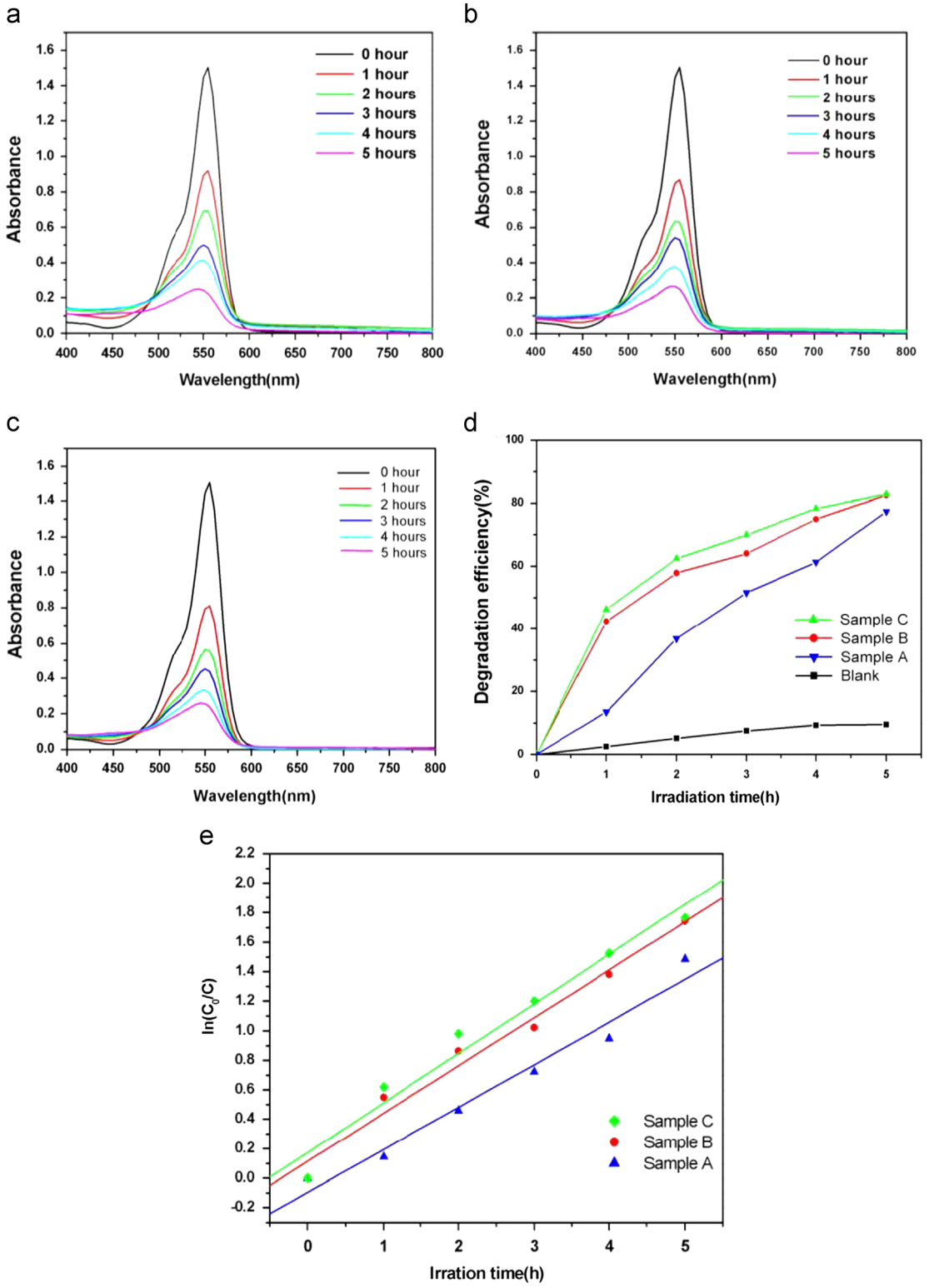

Fig. 6. (a)–(c) Adsorption changes of RhB aqueous in the presence of ZnSe NPs (Samples A–C) under irradiation with UV light at different intervals. (d) Degradation efficiency versus reaction time for ZnSe NPs (Samples A–C). (e) Plot of $\ln(C_0/C)$ as a function of UV irradiation time for the photocatalysis of RhB solution containing ZnSe NPs (Samples A–C).

Under laser excitation, the photogenerated electrons and holes will be created. But they will be separated and swept in opposite directions by the built-in electric field. For ZnSe NPs (21 nm), as shown in Fig. 4(a), the photogenerated electron–hole pairs created deeply within the bulk of ZnSe NPs (21 nm) have to diffuse through the bulk before reaching the surface depletion region. Since the photogenerated minority holes have a shorter diffusion length than the much more numerous majority electrons in ZnSe NPs (21 nm), all of them will radiatively recombine with electrons before they can reach the surface depletion region. Therefore, although the depletion region exists in ZnSe NPs (21 nm), as shown in Fig. 4(a), the chance of indirect recombination is quite smaller. So the direct radiative recombination in the bulk materials is the dominating recombination channel. On the contrary, in the case of ZnSe NPs (7 nm) as shown in Fig. 4(b), since the nanostructure will be thoroughly depleted, the photogenerated electrons and holes already in the surface depletion layer can be effectively separated and accumulated at the edge of conduction band and valence band without radiative recombination in the diffusion process.

Moreover, a defect-related emission band has a broad feature in the range 500–650 nm. Generally, the intensity ratio of NBE emission band to defect-related emission band is regarded as an indicator of the crystallinity of semiconductor materials [27]. The materials would have much better crystallization according to the larger intensity ratio. The relative PL intensity ratio of NBE emission (I_{NBE}) to defect-related emission (I_{DRE}) in our samples is estimated to be approximately 0.077, 0.495, and 3.649 corresponding to Samples C, B and A, respectively. The ratio of intensities I_{NBE}/I_{DRE} versus the reaction time is shown in Fig. 5. The Sample A has much better crystallization according to the larger intensity ratio. This difference in relative intensities can be attributed to the particle size and surface-to-volume ratio. The number of the surface atoms increased with decreasing size of the ZnSe NPs leading to the high surface state densities and defects [28]. The above mentioned results further confirmed the XRD and TEM results.

The photocatalytic activities of the ZnSe NPs (Samples A–C) with different particle sizes are evaluated in the degradation of well-known organic dye RhB. The RhB is a typical pollutant in the textile industry [29]. Fig. 6(a–c) displays the time-dependent UV–vis absorption spectra of RhB aqueous solution in the presence of the ZnSe NPs (Samples A–C) under exposure to UV light irradiation for various durations. Curves of degradation efficiency versus reaction time for ZnSe NPs (Samples A–C) are shown in Fig. 6 (d). The absorption peaks corresponding to RhB diminished gradually with increasing exposure time. The loss of absorbance indicates the destruction of the dye chromogen. Because no new peak is observed, the RhB is confirmed to be decomposed. When the RhB solution is exposed under UV light in the absence of any catalysts, the concentration changed slightly. Upon exposure to UV light for 5 h in the presence of ZnSe NPs with different particle sizes, RhB is found to degrade rapidly. The degradation kinetic of RhB under UV light irradiation is investigated by plotting the relationship between $\ln(C_0/C)$ and irradiation time (Fig. 6e). It can be seen that the curves of $\ln(C_0/C)$ versus irradiation time show linear lines, indicating a rather good correlation to first-order kinetics [20]. The ZnSe NPs (Sample C) show a slight better photocatalytic activity compared to the ZnSe NPs (Sample B). Moreover, the ZnSe NPs (Sample B) demonstrate superior photocatalytic activity over the ZnSe NPs (Sample A). One of the reasons may be that the particle size of ZnSe NPs varies with varying the reaction time. The particle size shows the following order: Sample C < Sample B < Sample A. Therefore, the surface to volume ratio of the ZnSe NPs shows the following order: Sample C > Sample B > Sample A. In general, the catalytic process is mainly caused by the adsorption and desorption of molecules on the surface of the catalyst [30,31]. The specific surface area plays an important role in the photocatalytic process, because the high specific surface area can provide more reactive adsorption/desorption sites for the photocatalytic reactions to occur [32,33]. The photocatalytic activity increases with the specific surface area increasing. So, the photocatalytic activity is higher when the nanoparticles have smaller particle size.

Furthermore, the PL analyses of the as-prepared ZnSe NPs may explain why ZnSe NPs (Sample C) show relatively high photocatalytic activity. Figs. 3(A) and 5 clearly show that the defect-related emission from the ZnSe NPs (Sample C) is relatively stronger than that of the ZnSe NPs (Samples B and A), which indicates more defects in the ZnSe NPs (Sample C). The low I_{NBE}/I_{DRE} ratio also indicates more defects in the NPs (Sample C). The photoelectrons and photoholes (electron–hole pairs) can be generated when semiconductor material is irradiated with a certain wavelength. It is generally accepted that the photocatalytic activity of semiconductor material can be increased with the amount of electron–hole pairs increasing. Meanwhile, the chance of generation and recombination of electron–hole pairs is equal. When photoelectrons are captured by defects in ZnSe NPs, the recombination of photoelectrons and photoholes can be effectively inhibited. Therefore, ZnSe NPs (Sample C) exhibit higher photocatalytic activity [34].

4. Conclusion

In summary, the low-toxic ZnSe NPs of different sizes from 7 to 21 nm were successfully synthesized by an easy controlled method. The as-prepared ZnSe NPs were zinc-blende structure, and the TEM images of the samples indicated that the NPs had uniform spherical shape. The room-temperature PL results showed that the NBE emission peak obviously red-shifted and the intensity decreased with decreasing particle size from 21 to 7 nm, and the ZnSe NPs (7 nm) showed a stronger and broader defect-related emission band. The ZnSe NPs with smaller particle size demonstrated higher photocatalytic activity compared to the NPs with larger particle size. And the photodegradation of Rhodamine B catalyzed by the ZnSe nanoparticles was a pseudo-first-order reaction.

Acknowledgments

This work was financially supported by the National Natural Science Foundation of China (Grant nos. 61178074, 61008051, 61378085), and Program for the development of

Science and Technology of Jilin province (Item nos. 201205078, 201215225).

References

[1] A. Aboulaich, M. Geszke, L. Balan, J. Ghanbaja, G. Medjahdi, R. Schneider, Inorg. Chem. 49 (2010) 10940–10948.
[2] Q. Zeng, S. Xue, S. Wu, K. Gan, L. Xu, J. Han, W. Zhou, R. Zou, Ceram. Int. 40 (2014) 2847–2852.
[3] X. Wang, L. Li, Yi. Lin, J. Zhu, Ceram. Int. 39 (2013) 5213–5218.
[4] W. Yan, C. Hu, Y. Xi, B. Wan, X. He, M. Zhang, Y. Zhang, Mater. Res. Bull. 44 (2009) 1205–1208.
[5] A.P. Pardo Gonzalez, H.G. Castro-Lora, L.D. López-Carreño, H. M. Martínez, N.J. Torres Salcedo, J. Phys. Chem. Solids 75 (2014) 713–725.
[6] Z. Chen, D. Wu, J. Lumin. 132 (2012) 2968–2974.
[7] S.L. Xiong, J.M. Shen, Q. Xie, Y.Q. Gao, Q. Tang, Y.T. Qian, Adv. Funct. Mater. 15 (2005) 1787–1792.
[8] S.Z. Wang, S.F. Yoon, L. He, X.C. Shen, J. Appl. Phys. 90 (2001) 2314–2320.
[9] H.Y. Lin, J.D. Wei, C.C. Ou, J.W. Lu, C.Y. Tsai, M.H. Lee, J. Alloys Compd. 509 (2011) 7009–7015.
[10] A.C. Deshpande, S.B. Singh, M.K. Abyaneh, R. Pasricha, S.K. Kulkarni, Mater. Lett. 62 (2008) 3803–3805.
[11] D. Han, C. Song, X. Li, Mater. Chem. Phys. 116 (2009) 41–45.
[12] S. Mahamuni, A.D. Lad, S. Patole, J. Phys. Chem. C 112 (2008) 2271–2277.
[13] S. Ramanathan, S. Patibandla, S. Bandyopadhyay, J. Anderson, J.D. Edwards, Nanotechnology 19 (2008) 19560–19567.
[14] B. Xi, D. Xu, S. Xiong, C. Wang, X. Feng, H. Zhou, Y. Qian, J. Phys. Chem. C 112 (2008) 5333–5338.
[15] Z. Zhu, G.D. Brownlie, P.J. Thompson, Appl. Phys. Lett. 67 (1995) 3762–3764.
[16] Z.S. Seddigi, Bull. Environ. Contam. Toxicol. 84 (2010) 564–567.
[17] S.H.S. Chan, T.Y. Wu, J.C. Juan, C.Y. Teh, J. Chem. Technol. Biotechnol. 86 (2011) 1130–1158.
[18] C. McCullagh, N. Skillen, M. Adams, P.K. Robertson, J. Chem. Technol. Biotechnol. 86 (2011) 1002–1017.
[19] S. Ekambaram, Y. Iikubo, A. Kudo, J. Alloys Compd. 433 (2007) 237–240.
[20] L. Chen, W. Zhang, C. Feng, Z. Yang, Y. Yang, Ind. Eng. Chem. Res. 51 (2012) 4208–4214.
[21] B. Feng, J. Yang, J. Cao, L. Yang, M. Gao, M. Wei, H. Zhai, Y. Sun, H. Song, J. Alloys Compd. 555 (2013) 241–245.
[22] Z.D. Hu, X.F. Duan, M. Gao, Q. Chen, L.M. Peng, J. Phys. Chem. C 111 (2007) 2987–2991.
[23] X. Zhang, Z. Liu, Q. Li, Y. Leung, K. Ip, S. Hark, Adv. Mater. 17 (2005) 1405–1410.
[24] U. Philipose, A. Saxena, H.E. Ruda, P.J. Simpson, Y.Q. Wang, K. L. Kavanagh, Nanotechnology 19 (2008) 215715–215720.
[25] Z.M. Liao, H.Z. Zhang, Y.B. Zhou, J. Xu, J.M. Zhang, D.P. Yu, Phys. Lett. A 372 (2008) 4505–4509.
[26] I. Shalish, H. Temkin, V. Narayanamurti, Phys. Rev. B 69 (2004) 245401–245404.
[27] L. Kumari, W.Z. Li, C.H. Vannoy, R.M. Leblanc, D.Z. Wang, Mater. Res. Bull. 45 (2010) 190–196.
[28] N.V. Bondar, J. Lumin. 130 (2010) 1–7.
[29] D. Gu, L. Huang, C. Shao, H. Fang, R. Zhang, H. Hou, Front. Chem. China 2 (2007) 436–441.
[30] T. Yao, Q. Zhao, Z. Qiao, F. Peng, H. Wang, H. Yu, C. Chi, J. Yang, Chem. Eur. J. 17 (2011) 8663–8670.
[31] L.L. Peng, T.F. Xie, Y.C. Lu, H.M. Fan, D.J. Wang, Phys. Chem. Chem. Phys. 12 (2010) 8033–8041.
[32] MS. Vohra, S. Kim, W. Choi, J. Photochem. Photobiol. A: Chem. 160 (2003) 55–60.
[33] F. Cao, W. Shi, L. Zhao, S. Song, J. Yang, Y. Lei, H. Zhang, J. Phys. Chem. C 112 (2008) 17095–17101.
[34] L.Q. Jing, Y.C. Qu, B.Q. Wang, S.D. Li, B.J. Jiang, L.B. Yang, W. Fu, H.G. Fu, J.Z. Sun, Sol. Energy Mater. Sol. Cells 90 (2006) 1773–1787.